Higher-order calculations

Giulia Zanderighi, Germán Rodrigo, Michele Treccani, Gábor Somogyi

The start-up of the LHC will usher in a new era of discovery in high-energy physics, with the machine operating at the highest centre-of-mass energy ever attained in the laboratory. In order to fully exploit its physics potential in Higgs and beyond the Standard Model (BSM) searches, a good understanding of the Standard Model is necessary. This requires a precise theoretical understanding of QCD.

The simplest description in exact perturbative calculations is at leading order (LO) using collinear factorization. Here, partons (or particles) should be well-separated and hard so as to avoid large soft-collinear corrections. Today, these LO calculations are fully automated. However, the drawback is that they have very large scale dependencies, enhanced sensitivities to kinematical cuts and a poor modelling of the jet structure (each parton corresponding to a jet). Therefore it is currently well appreciated that accurate predictions of QCD jet cross sections require the computation of radiative corrections at least to next-to-leading order (NLO) accuracy, first for SM processes, and BSM processes at a later stage. This is simply because the QCD coupling is not small and the phase space for emitting additional partons at the LHC is large, so that NLO corrections can be numerically significant. Benefits of NLO include a reduced dependence on unphysical scales, a better modelling of jets, and a more reliable control of the normalization and shape of cross sections.

Three ingredients are needed to compute a $2 \to N$ process at NLO: the real radiation of one parton from the $2 + N$ parton system (tree-level $2 + N + 1$ processes), one-loop virtual corrections to the $2 \to N$ process and a method to cancel the divergences of real and virtual corrections before numerical integration. The calculation of tree-level amplitudes has been automated and also the cancellation of divergences is, today, well understood [1–3]. Therefore up until very recently, the bottleneck at NLO has been the calculation of virtual, loop amplitudes.

In some cases however, NLO accuracy is not yet satisfactory and one would like to be able to calculate perturbative corrections beyond NLO. The physical situations when this happens have been discussed extensively in the literature [4]. Usually NLO is insufficient when the NLO correction is comparable to, or larger than, the LO result. This may happen when a process involves very different scales, so that large logarithms of the ratio of the two scales arise, which need to be resummed. This may also happen when new channels open up (at NLO those channels are effectively LO). This is the case, for instance, for b-jet production, where gluon splitting and flavour excitation processes enter at NLO and are enhanced by large logarithms. Also, gluon dominated processes are often characterized by large corrections, both because gluons radiate on average more than quarks and because of the steeply falling parton distribution functions (PDFs) at small x. NLO might also be insufficient if very high precision is useful. This is occasionally the case, for instance, in Drell-Yan processes, top pair production, and 3-jet production in e^+e^-. Finally, since NLO provides a first reliable estimate of cross sections, only NNLO can in principle provide a reliable error estimate of those cross sections. The bottleneck at NNLO is not the calculation of virtual matrix elements, as is the case at NLO, but rather the cancellation of divergences before numerical evaluation. In the following we will report on some recent progress in higher-order perturbative QCD.

1 One-loop amplitudes: the gluon case

Author: Giulia Zanderighi

Current and upcoming collider experiments require a good understanding of Standard Model (SM) processes in order to carry out any successful search for a Higgs or beyond SM signals (BSM). Therefore, these searches will benefit from next-to-leading order predictions, for SM processes first, and BSM processes at a later stage. Traditional Feynman diagram techniques, supplemented by robust numerical methods (Passarino-Veltman decomposition, Davydychev reduction, integration by part, tensor reduction) are well developed and made it possible to develop powerful computation tools [5–8] including procedures to handle potential numerical instabilities [7,9]. These techniques have been applied recently in a variety of $2 \to 3$ scattering processes and pushed to their limit in few $2 \to 4$ cases (see [10] for a recent review). The bottleneck of these approaches is the rapid increase both in the number of Feynman diagrams and in the number of terms generated during the tensors reduction. One promising alternative method is based on generalized unitarity [11]. Recent advances [12] allowed the development of analytic methods for the calculation of the full amplitude, including the rational part, using recursion relations [13,14]. A recent computational scheme is based on unitarity in integer higher dimension [15, 16]. This allows one to reduce the calculation of *full* one-loop amplitudes to the calculation of residues and of tree-level amplitudes involving complex momenta.

Using unitarity in higher integer dimension together with Berends-Giele recursion relations, we show that it is possible to develop an algorithm of mild, polynomial complexity for the evaluation of one-loop amplitudes. As a first application, we considered here pure gluonic amplitudes. We analyze the numerical stability of the results and the time dependence of the algorithm for virtual amplitudes with up to twenty external gluons.

1.1 The method

We [17] implemented the methods developed in Refs. [15, 16] with some minor modifications into the **Rocket** program. These methods build upon the formalism of Ref. [18] by removing the requirement of the four dimensional spinor language, thereby allowing for the extension of the method to D-dimensional cuts. To calculate the full one-loop N-gluon amplitude, it is sufficient to be able to calculate the leading colour ordered one-loop amplitude, since from these colour ordered amplitudes the full one-loop amplitude can be constructed [11, 19]. In the following we will therefore focus on the leading colour ordered amplitudes $A_N^{[1]}(1, 2, \ldots, N)$. We will use the (over-complete) master integral basis decomposition derived in Ref. [16]

$$
\begin{aligned}
A_N^{[1]} = &- \sum_{[i_1|i_5]} \frac{(D-4)}{2}\, e^{(2,0)}_{i_1 i_2 i_3 i_4 i_5}\, I^{(D+2)}_{i_1 i_2 i_3 i_4 i_5} \qquad (1)\\
&+ \sum_{[i_1|i_4]} \left(d^{(0,0)}_{i_1 i_2 i_3 i_4}\, I^{(D)}_{i_1 i_2 i_3 i_4} - \frac{(D-4)}{2}\, d^{(2,0)}_{i_1 i_2 i_3 i_4}\, I^{(D+2)}_{i_1 i_2 i_3 i_4} + \frac{(D-4)(D-2)}{4}\, d^{(4,0)}_{i_1 i_2 i_3 i_4}\, I^{(D+4)}_{i_1 i_2 i_3 i_4} \right)\\
&+ \sum_{[i_1|i_3]} \left(c^{(0,0)}_{i_1 i_2 i_3}\, I^{(D)}_{i_1 i_2 i_3} - \frac{(D-4)}{2} c^{(2,0)}_{i_1 i_2 i_3}\, I^{(D+2)}_{i_1 i_2 i_3} \right)\\
&+ \sum_{[i_1|i_2]} \left(b^{(0,0)}_{i_1 i_2}\, I^{(D)}_{i_1 i_2} - \frac{(D-4)}{2} b^{(2,0)}_{i_1 i_2}\, I^{(D+2)}_{i_1 i_2} \right) ,
\end{aligned}
$$

where we introduced the short-hand notation $[i_1|i_n] = 1 \leq i_1 < i_2 < \cdots < i_n \leq N$ and

$$
I^D_{i_1,\ldots i_N} = \int \frac{d^D l}{i\pi^{D/2}} \frac{1}{d_{i_1} d_{i_2} \ldots d_{i_N}} , \qquad d_i = d_i(l) = (l+q_i)^2 = (l+p_1+\cdots+p_i)^2 . \quad (2)
$$

Because some coefficients are multiplied with a dimensional factor $(D-4)$ they cannot be determined using four dimensional cuts, therefore we extend the dimensionality of the cut line to integer, higher dimensions, resulting in a well-defined on-shell particle after performing the cut [16]. By applying quintuple, quadruple, triple and double D_s-dimensional cuts (where $D_s \geq D$ denotes the dimensionality of the spin-space) we can determine the coefficients of the parametric form of the one-loop amplitude. This requires the calculation of the factorized unintegrated one-loop amplitude

$$
\begin{aligned}
\text{Res}_{i_1 \cdots i_M}(\mathcal{A}_N^{[1]}(l)) &= \left(d_{i_1} \times \cdots \times d_{i_M} \times \mathcal{A}_N^{[1]}(l) \right)_{d_{i_1} = \cdots = d_{i_M} = 0} \\
&= \sum_{\{\lambda_1,\ldots,\lambda_M\}=1}^{D_s-2} \left(\prod_{k=1}^{M} \mathcal{A}^{[0]}_{i_{k+1}-i_k}(l^{(\lambda_k)}_{i_k}, p_{i_k+1}, \ldots, p_{i_{k+1}}, -l^{(\lambda_{k+1})}_{i_{k+1}}) \right) , \quad (3)
\end{aligned}
$$

where $M \leq 5$ and the D-dimensional loop momentum l has to be chosen such that $d_{i_1}(l) = \cdots = d_{i_M}(l) = 0$. To calculate these tree amplitudes we use the standard Berends-Giele recursion relation [20] which is valid in arbitrary dimension and for complex momenta. The generic solution for the loop momentum in Eq. (3) is given by

$$
l^\mu_{i_1 \cdots i_M} = V^\mu_{i_1 \cdots i_M} + \sqrt{\frac{-V^2_{i_1 \cdots i_M}}{\alpha_M^2 + \cdots + \alpha_D^2}} \left(\sum_{i=M}^{D} \alpha_i\, n_i^\mu \right) , \qquad (4)
$$

for arbitrary values of the variables α_i. The vector $V^\mu_{i_1 \cdots i_m}$ is defined in the space spanned by the denominator offset momenta $\{q_{i_1}, \ldots, q_{i_M}\}$, while the orthonormal basis vectors $\{n^\mu_M, \ldots, n^\mu_D\}$ span the space orthogonal to the space spanned by these momenta [15, 16]. Given the solution to the on-shell conditions $l^\mu_{i_1 \cdots i_M}$ in Eq. (4), the loop momenta flowing into the tree amplitudes l_{i_k} and $l_{i_{k+1}}$ in Eq. (3) are fixed by momentum conservation (see Ref. [15]). Once all coefficients

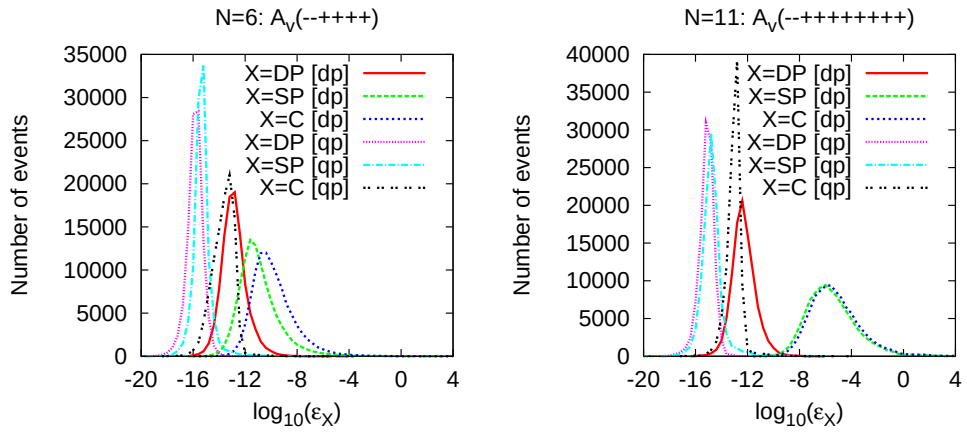

Fig. 1: Accuracy on the double pole, single pole and constant part of the maximally helicity violating (MHV) amplitude with adjacent negative helicities for 6 up to 11 external gluons. Double ([dp]) and quadrupole ([qp]) precision results for 100,000 phase space points are shown. Refer to the text for more details.

in Eq. (1) have been determined we can continue the dimensionality to the non-integer limit: $D \to 4 - 2\epsilon$. Neglecting terms of order ϵ we find for the colour ordered one-loop amplitude

$$A_N^{[1]} = \sum_{[i_1|i_4]} d^{(0,0)}_{i_1 i_2 i_3 i_4} \, I^{(4-2\epsilon)}_{i_1 i_2 i_3 i_4} + \sum_{[i_1|i_3]} c^{(0,0)}_{i_1 i_2 i_3} \, I^{(4-2\epsilon)}_{i_1 i_2 i_3} + \sum_{[i_1|i_2]} b^{(0,0)}_{i_1 i_2} \, I^{(4-2\epsilon)}_{i_1 i_2}$$
$$- \sum_{[i_1|i_4]} \frac{d^{(4,0)}_{i_1 i_2 i_3 i_4}}{6} + \sum_{[i_1|i_3]} \frac{c^{(2,0)}_{i_1 i_2 i_3}}{2} - \sum_{[i_1|i_2]} \frac{(q_{i_1} - q_{i_2})^2}{6} b^{(2,0)}_{i_1 i_2} + \mathcal{O}(\epsilon) \, . \tag{5}$$

The terms in the first line give rise to the so-called cut-constructable part of the amplitude [21]. The terms in the second line can be identified with the rational part. In the approach used here the division between these two contributions is irrelevant. For the numerical evaluation of the bubble, triangle and box master integrals we use the package developed in Ref. [22].

1.2 Numerical results: accuracy and time dependence of the algorithm

To study the numerical accuracy of the on-shell method implemented in **Rocket** we define

$$\varepsilon_C = \log_{10} \frac{|A_N^{\mathrm{v,unit}} - A_N^{\mathrm{v,anly}}|}{|A_N^{\mathrm{v,anly}}|} \, , \tag{6}$$

where "unit" denotes the result obtained with the on-shell method and "anly" the analytical result for the constant parts of the one-loop helicity amplitudes (or in the case of $N = 6$ the numerical results of [23]). Similarly, we denote by $\varepsilon_{\mathrm{DP}}$ and $\varepsilon_{\mathrm{SP}}$ the accuracy on the double and single poles, respectively.

In Fig. (1) we show the accuracy for the two adjacent minus helicity gluon MHV one-loop amplitudes, $A_N^{[1]}(--+\cdots+)$, for $N = 6$ and $N = 11$, which are known analytically [11,21,24].

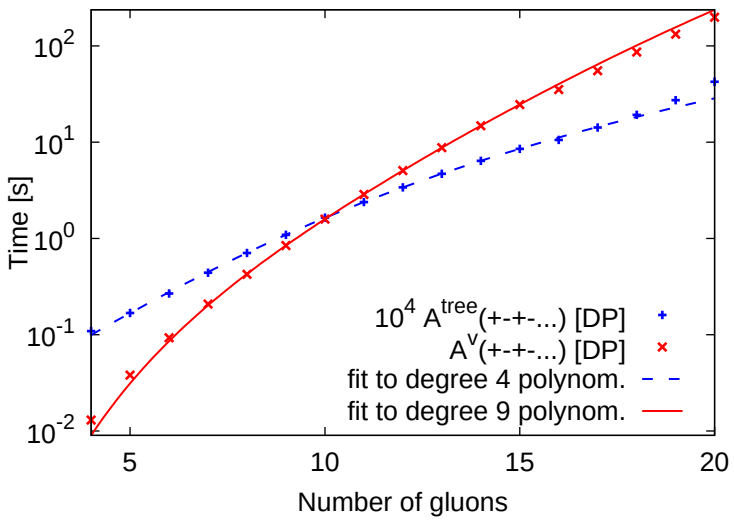

Fig. 2: Time in seconds needed to compute tree (blue, dashed) and one-loop (red, solid) ordered amplitudes with gluons of alternating helicity signs, $A_N^{[1]}(+-+-+...)$, as a function of the number of external gluons ranging between 4 to 20 using a single 2.33 GHz Xeon processor.

The 100,000 phase space points used for each multiplicity are generated uniformly in phase space using the Rambo algorithm [25] imposing minimal cuts. We plot the accuracy for the double pole ($\mathrm{X} = \mathrm{DP}[\mathrm{dp}]$, solid, red), the single pole ($\mathrm{X} = \mathrm{SP}[\mathrm{dp}]$, green, dot-dashed) and the constant part ($\mathrm{X} = \mathrm{C}[\mathrm{dp}]$, blue, dotted). We see that an excellent accuracy can be reached for all contributions. The tail of the distribution reaching to large values of ϵ contains only a very few points. This lack of agreement is due to numerical instabilities due to vanishing Gram determinants or other small intermediate denominators. Several techniques have been developed to deal with such exceptional points, such as developing systematic expansions [6, 7, 9] or interpolating across the singular regions [26]. We adopt here a more brute force approach and recur to quadrupole precision. In Fig. (1), we see three more curves marked $[\mathrm{qp}]$: they correspond to the numerical accuracy on the same phase space points when the one-loop amplitude is computed in quadrupole precision. Out of 100,000 phase space points sampled, not a single one has an accuracy worse than 10^{-4} and, at quadrupole precision we see no appreciable worsening of the accuracy with increasing N. Therefore up to $N = 11$ (and probably even for more gluons) quadrupole precision is sufficient to guarantee an accuracy needed for any next-to-leading order QCD correction. If higher precision is desired one can choose to evaluate the few phase space points which have insufficient precision using some arbitrary precision package, at the cost of higher computation time. We note that while the plots here presented are for the MHV amplitudes, we performed a similar study for the finite amplitudes ($A_N^{[1]}(+\cdots+)$, $A_N^{[1]}(-+\cdots+)$) and obtain very similar results. This indicates that the accuracy is essentially independent of the helicities of the external gluons.

A very important property of this method is that the time needed to compute one-loop amplitudes does not grow factorially with the number of external legs; indeed it is straightforward

to estimate the scaling of time with the number of gluons N. The calculation of tree-level amplitudes computed via Berends-Giele recursion relations with caching of previously computed amplitudes requires a time which grows as $\tau_{\rm tree,N} \propto N^4$ [27]. The total number of tree amplitudes that one needs to evaluate to get a one-loop amplitudes is given by

$$\begin{aligned} n_{\rm tree} &= \left\{(D_{s_1}-2)^2+(D_{s_2}-2)^2\right\} \\ &\times \left(5\,c_{5,\max}\binom{N}{5}+4\,c_{4,\max}\binom{N}{4}+3\,c_{3,\max}\binom{N}{3}+2\,c_{2,\max}\left[\binom{N}{2}-N\right]\right), \end{aligned} \tag{7}$$

where the first factor is due to the sum over polarization of the internal cut gluons in two integer dimensions D_{s_1} and D_{s_2}. The constants $c_{m,\max}$ denote the number of times one needs to perform a multiple cut in order to fully constrain the system of equations determining the master integral coefficients. Explicitly one has have $c_{5,\max}=1$, $c_{4,\max}=5$, $c_{3,\max}=10$, and $c_{2,\max}=10$. The integer number in front counts the number of tree amplitudes per multiple cut, finally the binomial coefficients corresponds to the number of possible cuts (for two point functions we subtract the vanishing contributions of the external self energy graphs). It follows that the time needed to evaluate a one-loop ordered amplitude will for large N scale as

$$\tau_{\rm one-loop,N} \sim n_{\rm tree}\cdot\tau_{\rm tree,N} \propto N^9\,. \tag{8}$$

In Fig. (2) we plot the time needed to compute tree (blue, dashed) and one-loop (red, solid) ordered amplitudes with alternating helicity signs for the gluons, $A_N^{[1]}(+-+-\ldots)$, as a function of the number of gluons in the range between four and twenty. Time estimates refer to using a 2.33 GHz Xeon processor. One can see that the times needed to compute tree and one-loop ordered amplitudes are consistent with a N^4 and N^9 growth respectively. When running in quadrupole precision rather than in double precision the evaluation time grows, but the scaling with N remains unchanged. Finally we remark that the time is independent on the helicities of the external gluons.

1.3 Discussion and outlook

The results presented here are based on D-dimensional unitarity implemented in the Fortran 90 code **Rocket**. The very mild, power-like increase in computational time and the numerical stability of the results demonstrate the power of this approach. The large number of gluons considered here demonstrates that the gluon case is fully solved as far as virtual amplitudes are concerned.

Recently this method has been applied also to other processes $0 \to t\bar{t}ggg$ [28], $0 \to q\bar{q}W$+n gluons and $0 \to q\bar{q}\bar{Q}QW$ + 1 gluon [29]. These recent calculations demonstrate the generality of the approach and constitute first steps towards automated one-loop calculations.

2 Duality relation between one-loop integrals and single-cut phase-space integrals

Author: Germán Rodrigo

As discussed in Sec. , the physics program of the LHC requires the evaluation of multi-leg signal and background processes at next-to-leading order (NLO). In the recent years, important efforts have been devoted to the calculation of many $2 \to 3$ processes and some $2 \to 4$ processes (see, e.g., [10]).

We have recently proposed a method [30–32] to numerically compute multi-leg one-loop cross sections in perturbative field theories. The starting point of the method is a duality relation between one-loop integrals and phase-space integrals. The duality relation requires to properly regularize propagators by a complex Lorentz-covariant prescription, which is different from the customary $+i0$ prescription of the Feynman propagators. This duality relation has analogies with the Feynman's Tree Theorem (FTT) [33], but involves only single cuts of the one-loop Feynman diagrams.

The duality relation between one-loop integrals and single-cut phase-space integrals is obtained [32] by applying the Cauchy residue theorem to a generic one-loop integral $L^{(N)}$:

$$L^{(N)}(p_1, p_2, \ldots, p_N) = \int_q \prod_{i=1}^{N} G(q_i) \,, \qquad \int_q \cdots \equiv -i \int \frac{d^d q}{(2\pi)^d} \, \ldots \,, \tag{9}$$

where $q_i = q + \sum_{k=1}^{i} p_k$ are the momenta of the internal lines, with q the loop momentum, and p_i ($\sum_{i=1}^{N} p_i = 0$) the external (outgoing and clockwise ordered) momenta, and G is the customary Feynman propagator, which for massless internal lines is given by

$$G(q) \equiv \frac{1}{q^2 + i0} \,. \tag{10}$$

In the complex plane of the loop energy q_0 the Feynman propagator has two poles; the pole with positive (negative) energy is slightly displaced below (above) the real axis. Hence, by using the Cauchy residue theorem in the q_0 complex plane, with the integration contour closed at ∞ in the lower half-plane, we obtain

$$L^{(N)}(p_1, p_2, \ldots, p_N) = -2\pi i \int_{\mathbf{q}} \sum \mathrm{Res}_{\{\mathrm{Im}\, q_0 < 0\}} \left[\prod_{i=1}^{N} G(q_i) \right] \,. \tag{11}$$

The Feynman propagators produce N poles in the lower half-plane that contribute to the residues in Eq. (11). The calculation of these residues is elementary, but it involves several subtleties. We get

$$\mathrm{Res}_{\{i^{\mathrm{th}}\mathrm{pole}\}} \frac{1}{q_i^2 + i0} = \int dq_0 \; \delta_+(q_i^2) \,. \tag{12}$$

This result shows that considering the residue of the Feynman propagator of the internal line with momentum q_i is equivalent to cutting that line by including the corresponding on-shell propagator $\delta_+(q_i^2)$. The other propagators $G(q_j)$, with $j \neq i$, which are not singular at the value of the pole of $G(q_i)$, contribute as follows [32]:

$$\prod_{j \neq i} \frac{1}{q_j^2 + i0} \bigg|_{q_i^2 = -i0} = \prod_{j \neq i} \frac{1}{q_j^2 - i0\, \eta(q_j - q_i)} \,, \tag{13}$$

where η is a future-like vector, i.e. a d-dimensional vector that can be either light-like ($\eta^2 = 0$) or time-like ($\eta^2 > 0$) with positive definite energy ($\eta_0 \geq 0$). The calculation of the residue at the pole of the i^{th} internal line modifies the $i0$ prescription of the propagators of the other

internal lines of the loop. This modified regularization is named 'dual' $i0$ prescription, and the corresponding propagators are named 'dual' propagators. The dual prescription arises from the fact that the original Feynman propagator $1/(q_j^2 + i0)$ is evaluated at the *complex* value of the loop momentum q, which is determined by the location of the pole at $q_i^2 + i0 = 0$. The presence of η is a consequence of the fact that the residue at each of the poles is not a Lorentz-invariant quantity, because a given system of coordinates has to be specified to apply the residue theorem. Different choices of the future-like vector η are equivalent to different choices of the coordinate system. The Lorentz-invariance of the loop integral is, however, recovered after summing over all the residues.

Inserting the results of Eqs. (12)-(13) in Eq. (11) gives us the duality relation between one-loop integrals and single-cut phase-space integrals [32]:

$$L^{(N)} = -\,\widetilde{L}^{(N)}\,, \tag{14}$$

where the explicit expression of the phase-space integral $\widetilde{L}^{(N)}$ is

$$\widetilde{L}^{(N)}(p_1, p_2, \ldots, p_N) = \int_q \sum_{i=1}^{N} \widetilde{\delta}(q_i) \prod_{\substack{j=1 \\ j\neq i}}^{N} \frac{1}{q_j^2 - i0\,\eta(q_j - q_i)}\,, \tag{15}$$

with $\widetilde{\delta}(q) \equiv 2\pi i\,\delta_+(q^2)$. Contrary to the FTT, the duality relation involves single-cut contributions only. This result is achieved by replacing the Feynman propagators in $L^{(N)}$ by dual propagators in $\widetilde{L}^{(N)}$, which depend on the auxiliary vector η. However, $\widetilde{L}^{(N)}$ does not depend on η, provided it is fixed to be the same in all its contributing single-cut terms (dual integrals). The duality relation, therefore, directly expresses the one-loop integral as the phase-space integral of a tree-level quantity. In the case of the FTT, the relation between loop and tree-level quantities is more involved, since the multiple-cut contributions contain integrals of expressions that correspond to the product of m tree-level diagrams over the phase-space for different number of particles.

The FTT and the duality theorem can be directly related starting from a basic identity between dual and Feynman propagators [32]:

$$\widetilde{\delta}(q)\,\frac{1}{2qk + k^2 - i0\,\eta k} = \widetilde{\delta}(q)\,\Big[G(q+k) + \theta(\eta k)\,\widetilde{\delta}(q+k)\Big]\,. \tag{16}$$

This identity applies to the dual propagators when they are inserted in a single-cut integral. The proof of equivalence of the FTT and the duality theorem is purely algebraic [32]. We explicitly illustrate it by considering the massless two-point function $L^{(2)}(p_1, p_2)$. Its dual representation is

$$\widetilde{L}^{(2)}(p_1, p_2) = \int_q \widetilde{\delta}(q) \left(\frac{1}{2qp_1 + p_1^2 - i0\,\eta p_1} + (p_1 \leftrightarrow p_2)\right)\,. \tag{17}$$

Inserting Eq. (16) in Eq. (17), we obtain

$$\widetilde{L}^{(2)}(p_1, p_2) = L^{(2)}_{1-\mathrm{cut}}(p_1, p_2) + [\theta(\eta p_1) + \theta(\eta p_2)]\; L^{(2)}_{2-\mathrm{cut}}(p_1, p_2)\,, \tag{18}$$

where the m-cut integrals $L^{(2)}_{m-\mathrm{cut}}$ are the contributions with precisely m delta functions:

$$L^{(2)}_{1-\mathrm{cut}}(p_1,p_2) = \int_q \widetilde{\delta}(q)\,(G(q+p_1)+G(q+p_2))\ , \qquad L^{(2)}_{2-\mathrm{cut}}(p_1,p_2) = \int_q \widetilde{\delta}(q)\,\widetilde{\delta}(q+p_1)\ . \tag{19}$$

Owing to momentum conservation (namely, $p_1+p_2=0$), $\theta(\eta p_1)+\theta(\eta p_2)=1$, and then the dual and the FTT representations of the two-point function are equivalent. The proof of equivalence in the case of higher N-point functions proceeds in a similar way [32], the key ingredient simply being the constraint of *momentum conservation*.

The extension of the duality relation to include propagators with real finite masses M_i is straightforward. The massless on-shell delta function $\widetilde{\delta}(q_i)$ is replaced by $\widetilde{\delta}(q_i;M_i) = 2\pi\, i\ \delta_+(q_i^2 - M_i^2)$ when a massive loop internal line is cut to obtain the dual representation. The $i0$ prescription of the dual propagators is not affected by real masses. The corresponding dual propagator is

$$\frac{1}{q_j^2 - M_j^2 - i0\,\eta(q_j-q_i)}\ . \tag{20}$$

Unstable particles, in contrast, introduce a finite imaginary contribution in their propagators. The form of the complex-mass propagators is scheme dependent, but their poles in the q_0 complex plane are located at a finite imaginary distance from the real axis. Then, when complex-mass propagators are cut in the duality relation, the $+i0$ prescription of the usual Feynman propagators can be removed.

The polarization tensor of a spin-one gauge boson has in general the form

$$d^{\mu\nu}(q) = -g^{\mu\nu} + (\zeta-1)\ \ell^{\mu\nu}(q)\,G_G(q)\ . \tag{21}$$

The second term on the right-hand side is absent only in the 't Hooft–Feynman gauge ($\zeta=1$). The tensor $\ell^{\mu\nu}(q)$, which propagates longitudinal polarizations, has a polynomial dependence on the momentum q and, therefore, it does not interfere with the residue theorem. The factor $G_G(q)$ ('gauge-mode' propagator), however, can introduce extra unphysical poles (i.e. in addition to the poles of the associated Feynman propagator) that will modify the duality relation. Apart from the 't Hooft–Feynman gauge, the duality relation in the form presented here, i.e. with the inclusion of the sole single-cut terms from the Feynman propagators, turns out to be valid [32] in spontaneously-broken gauge theories in the unitary gauge, and in unbroken gauge theories in physical gauges specified by a gauge vector n^ν, *provided* the dual vector η^μ is chosen such that $n\cdot\eta = 0$. This excludes gauges where n^ν is time-like. In any other gauge, additional single-cut terms from the absorptive contribution of the unphysical gauge poles have to be introduced in the duality relation.

The duality relation can be applied to evaluate not only basic one-loop integrals $L^{(N)}$ but also complete one-loop quantities $\mathcal{A}^{(1-\mathrm{loop})}$ (such as Green's functions and scattering amplitudes). The analogue of Eqs. (14) and (15) is the following duality relation [32]:

$$\mathcal{A}^{(1-\mathrm{loop})} = -\ \widetilde{\mathcal{A}}^{(1-\mathrm{loop})}\ . \tag{22}$$

The expression $\widetilde{\mathcal{A}}^{(1-\mathrm{loop})}$ on the right-hand side is obtained from $\mathcal{A}^{(1-\mathrm{loop})}$ in the same way as $\widetilde{L}^{(N)}$ is obtained from $L^{(N)}$: starting from any Feynman diagram in $\mathcal{A}^{(1-\mathrm{loop})}$, and considering

all possible replacements of each Feynman propagator $G(q_i)$ in the loop with the cut propagator $\widetilde{\delta}(q_i; M_i)$, and then replacing the uncut Feynman propagators with dual propagators. All the other factors in the Feynman diagrams are left unchanged in going from $\mathcal{A}^{(1-\mathrm{loop})}$ to $\widetilde{\mathcal{A}}^{(1-\mathrm{loop})}$.

Equation (22) establishes a correspondence between the one-loop Feynman diagrams contributing to $\mathcal{A}^{(1-\mathrm{loop})}$ and the tree-level Feynman diagrams contributing to the phase-space integral in $\widetilde{\mathcal{A}}^{(1-\mathrm{loop})}$. How are these tree-level Feynman diagrams related to those contributing to the tree-level expression $\mathcal{A}^{(\mathrm{tree})}$, i.e. the tree-level counterpart of $\mathcal{A}^{(1-\mathrm{loop})}$? The answer to this question is mainly a matter of combinatorics of Feynman diagrams. If $\mathcal{A}^{(1-\mathrm{loop})}$ is an off-shell Green's function, the phase-space integrand in $\widetilde{\mathcal{A}}^{(1-\mathrm{loop})}$ is directly related to $\mathcal{A}^{(\mathrm{tree})}$ [32]. In a sketchy form, we can write:

$$\mathcal{A}_N^{(1-\mathrm{loop})}(\dots) \sim \int_q \sum_P \tilde{\delta}(q; M_P)\, \widetilde{\mathcal{A}}_{N+2}^{(\mathrm{tree})}(q, -q, \dots)\,, \tag{23}$$

where $\sum_P$ denotes the sum over all the types of particles and antiparticles that can propagate in the loop internal lines, and $\widetilde{\mathcal{A}}^{(\mathrm{tree})}$ simply differs from $\mathcal{A}^{(\mathrm{tree})}$ by the replacement of dual and Feynman propagators. The extension of Eq. (23) to scattering amplitudes requires a careful treatment of the on-shell limit of the corresponding Green's functions [32].

In recent years much progress [20, 34–40] has been achieved on the computation of tree-level amplitudes, including results in compact analytic form. Using the duality relation, this amount of information at the tree level can be exploited for applications to analytic calculations at the one-loop level.

The computation of cross sections at next-to-leading order (NLO) requires the separate evaluation of real and virtual radiative corrections. Real (virtual) radiative corrections are given by multi-leg tree-level (one-loop) matrix elements to be integrated over the multiparticle phase-space of the physical process. The loop–tree duality discussed here, as well as other methods that relate one-loop and phase-space integrals, have an attractive feature [30, 41–44]: they recast the virtual radiative corrections in a form that closely parallels the contribution of the real radiative corrections. This close correspondence can help to directly combine real and virtual contributions to NLO cross sections. In particular, using the duality relation, we can apply [30] mixed analytical/numerical techniques to the evaluation of the one-loop virtual contributions. The (infrared or ultraviolet) divergent part of the corresponding dual integrals can be analytically evaluated in dimensional regularization. The finite part of the dual integrals can be computed numerically, together with the finite part of the real emission contribution. Partial results along these lines are presented in Refs. [30, 31] and further work is in progress. The extension of the duality relation from one-loop to two-loop Feynman diagrams is also under investigation.

3 Monte Carlo simulations of $t\bar{t}$ + jets at hadron colliders

Author: Michele Treccani

Because of the high energy of the Tevatron and the LHC, one of the most interesting fields refers to the class of events with multiple final states, giving rise to multiple jets with complicated topologies. There exist different strategies to tackle this problem, with distinct features and points of strength. The main problem is how to consistently compose the contributions due to Matrix Element (ME) calculations with the contributions of the Monte Carlo (MC) showering codes, in

order to exploit their complementarity and avoid at the same time the so-called double counting phenomenon [45–48].
We will here focus on a particular approach which relies on a consistent leading-logarithmic (LL) accuracy in the prediction of a final state F accompanied by a varying number of extra jets. The double counting is avoided adopting a so-called *matching algorithm* for matrix elements and parton shower. We study in detail the *MLM* matching [49–51] embedded in the the ME generator ALPGEN [52] in order to describe the $t\bar{t}$ pair production at hadron colliders. First we will address its stability with respect to its internal parameters by comparing predictions obtained with different parameters.
In a step further, we will perform detailed numerical comparison between *MLM* matching and MC program MC@NLO which is an alternative strategy to cope with double counting and reaches next-to-leading order (NLO) accuracy in the prediction [53–55].

3.1 Consistency studies of the matching algorithm

In this section we study the overall consistency of the matching algorithm applied to the case of $t\bar{t}$ final states. We shall consider $t\bar{t}$ production at the Tevatron ($p\bar{p}$ collisions at $\sqrt{s} = 1.96$ TeV) and at the LHC (pp collisions at $\sqrt{s} = 14$ TeV).
The generation parameters for the light partons are defined by the following kinematical cuts: the default values for the event samples at the Tevatron (LHC) are given by: p_T^{min}=20 (30) $\mathrm{GeV}$and R_{min}=0.7 (0.7), while they are considered only in the geometrical region defined by $\eta \leq 4(5)$.
The top particle is assumed to be stable, and therefore all jets coming from the decay of top quarks are neglected. For the shower evolution we use HERWIG, version 6.510 [56–58]. We stopped the evolution after the perturbative phase, in order to drop down all the common systematics that could smooth out any possible discrepancy between the various simulations. For all generations we chose the parton distribution function set MRST2001J [59], with renormalization and factorization scales squared set equal to:

$$\mu_{\mathrm{R}}^2 = \mu_{\mathrm{F}}^2 = \sum_{i=t,\bar{t},\mathrm{jets}} [m_i^2 + (p_T^i)^2].$$

Jet observables are built out of the partons emerging form the shower in the rapidity range $|\eta| \leq 6$ and adopting the cone algorithm GETJET [60]. The jet cone size is set to $R_{cone} = 0.7$ and the minimum transverse momentum to define a jet at the Tevatron(LHC) is 15(20) GeV .
To our analysis, the important feature of the whole procedure is the presence of two set of parameters: the generation cuts and the matching cuts (see [49–51]). The first set is necessary to avoid the infrared (IR) and collinear singularities: p_T^{min}, the minimum transverse momentum of the extra parton(s) to be generated, and R_{min}, the minimum separation between extra-partons in the (η, ϕ) plane. Along with these parameters, there exist an analogous set, but with slightly different meaninings : the matching cuts E_T^{clus} and R_{match}.
We choose two independent variations of the generation and of two of the matching cuts, while keeping fixed our definition of the physical objects (the jets) and of the observables. In both cases, we find that these distribution are stable against reasonable variations of the internal parameters, with relative differencies confined well below few percents.
Angular observables, such as ΔR between jets, are more sensible, since they are directly related to the matching variables, nevertheless their agreement is within 10%.
The analysis at the LHC, which will not be shown here, leads to qualitatively and quantitatively similar results.

3.2 Comparisons with MC@NLO

We shall now compare in detail the description of $t\bar{t}$ events as provided by ALPGEN and MC@NLO. For consistency with the MC@NLO approach, where only the $\mathcal{O}(\alpha_s^3)$ ME effects are included, we use ALPGEN samples obtained by stopping the ME contributions only to 1 extra-parton besides the $t\bar{t}$ pair. This strategy allow to highlight the different features of the two alternative approaches applied to same set of contributions. It is understood that a homogeneous comparison can only be done through the introduction of a proper K-factor, determined by the ratio of the total rates of the two predictions. We adopt the same simulation setup as before, modifying only the same factorization and renormalization scale in order to match MC@NLO's default:

$$\mu_{\rm R}^2 = \mu_{\rm F}^2 = \sum_{i=t,\bar{t}} \frac{1}{2}[m_i^2 + (p_T^i)^2].$$

The upper two rows of plots in Fig. 3 refer to inclusive properties of the $t\bar{t}$ system, namely the transverse momentum and rapidity of the top and anti-top quark, the transverse momentum of the $t\bar{t}$ pair, and the azimuthal angle $\Delta\phi^{t\bar{t}}$ between the top and anti-top quark. The overall agreement is good, once ALPGEN is corrected with the proper K-factor (1.36 for the Tevatron, and 1.51 for the LHC), and no large discrepancy is seen between the two descriptions of the chosen distributions. The most significant differencies (10 to 20%) are seen in the p_T^{top} distribution, ALPGEN's one being slightly softer.

In jet-related quantities, while the p_T of leading and sub-leading jets agree, instead the rapidity of the leading jet reveals two distinct patterns: MC@NLO predictions show a dip at $y_1 = 0$, which is not present in ALPGEN predictions. This difference is particularly marked at the Tevatron, but is very visible also at the LHC. This is shown in the right figure of the third row in Fig. 3. Visible differences are also present in the distribution of the first and second jet separation in (η, ϕ) space, $\Delta R_{1,2}$. To understand the difference in the rapidity distribution, we look in more detail in Fig. 4 at some features in the MC@NLO description of the leading jet. For the p_T of the leading jet, $p_{T,1}$, we plot separately the contribution from the various components of the MC@NLO generation: events in which the shower is initiated by the LO $t\bar{t}$ hard process, and events in which the shower is initiated by a $t\bar{t} + q(g)$ hard process. In the latter we separate the contribution of positive- and negative-weight events, where the distribution of negative events is shown in absolute value. The plots show that for MC@NLO the contribution of the $t\bar{t} + q(g)$ hard process is almost negligible over most of the relevant range and becomes appreciable only for very large values of $p_{T,1}$. This hierarchy is stronger at the LHC than at the Tevatron.

Upper set of Fig. 5 shows the various contributions to the rapidity distribution y_1 for different jet p_T thresholds. It appears that the y_1 distribution resulting from the shower evolution of the $t\bar{t}$ events in MC@NLO has a strong dip at y_1=0, a dip that cannot be compensated by the more central distributions of the jet from the $t\bar{t} + q(g)$ hard process, given its marginal role in the overall jet rate.

That the dip at y_1=0 is a feature typical of jet emission from the $t\bar{t}$ state in HERWIG is shown in central set of Fig. 5, obtained from the standard HERWIG code rather than from MC@NLO. We speculate that this feature is a consequence of the dead-cone description of hard emission from heavy quarks implemented in the HERWIG shower algorithm. To complete our analysis, we show in lower set of Fig. 5 the comparison between the ALPGEN, MC@NLO and the parton-level y_1 spectra, for different jet p_T thresholds. We notice that at large p_T, where the Sudakov effects that induce potential differences between the shower and the PL results have vanished, the ALP-

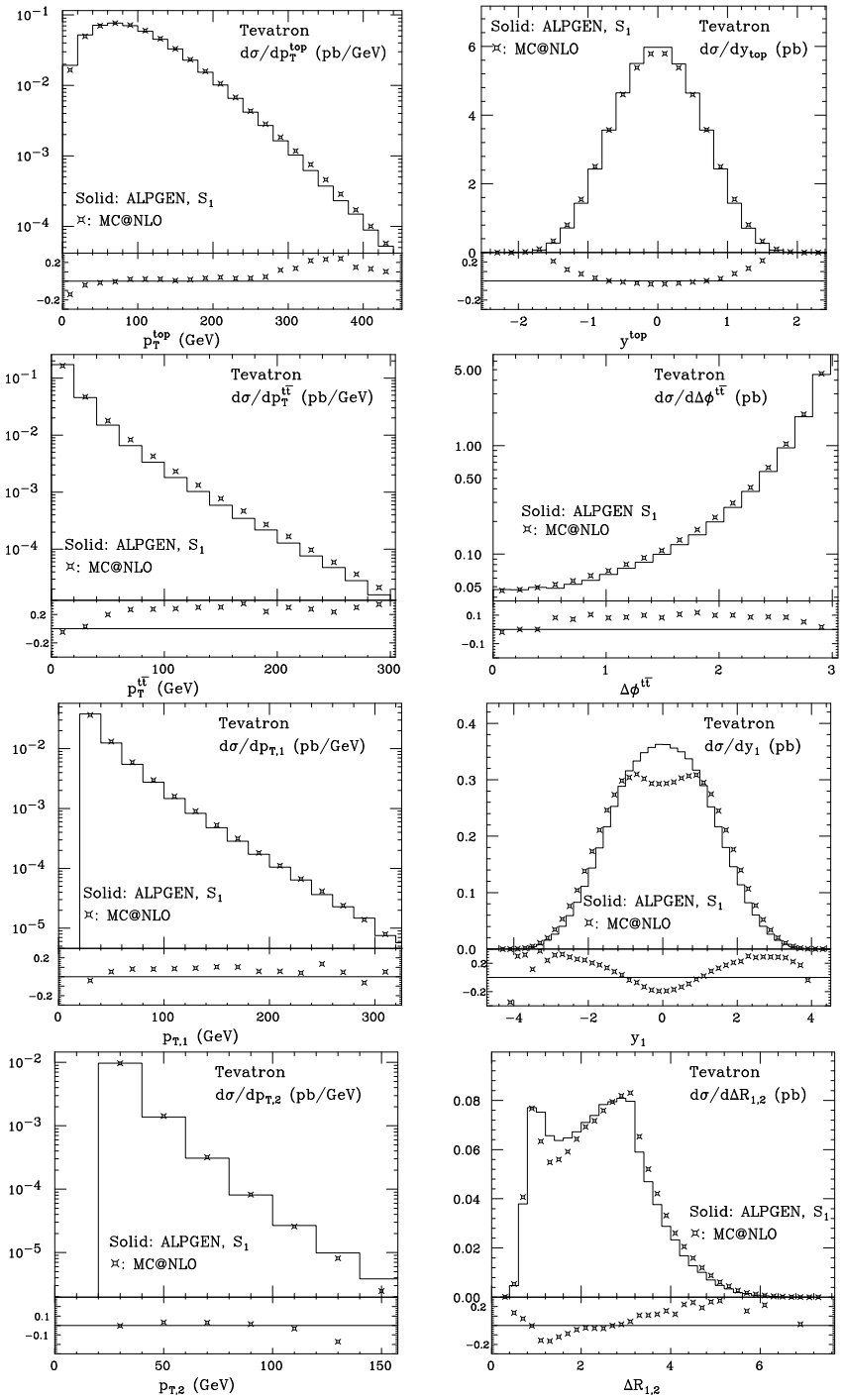

Fig. 3: Comparison of ALPGEN (histogram) and MC@NLO (plot) distributions, at the Tevatron. The ALPGEN results are rescaled to MC@NLO, using the K factor of 1.36. The relative difference (MC@NLO-ALPGEN)/ALPGEN) is shown at the bottom of each plot.

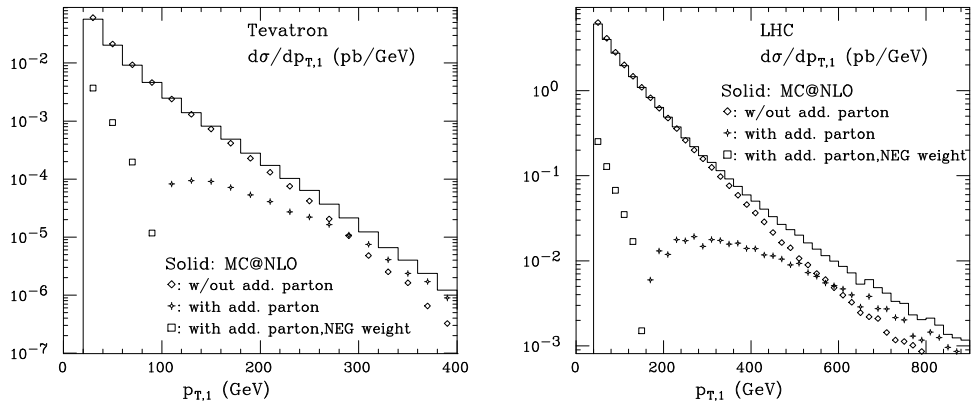

Fig. 4: Contributions to the transverse momentum of the leading jet in MC@NLO. Tevatron (left) and LHC (right).

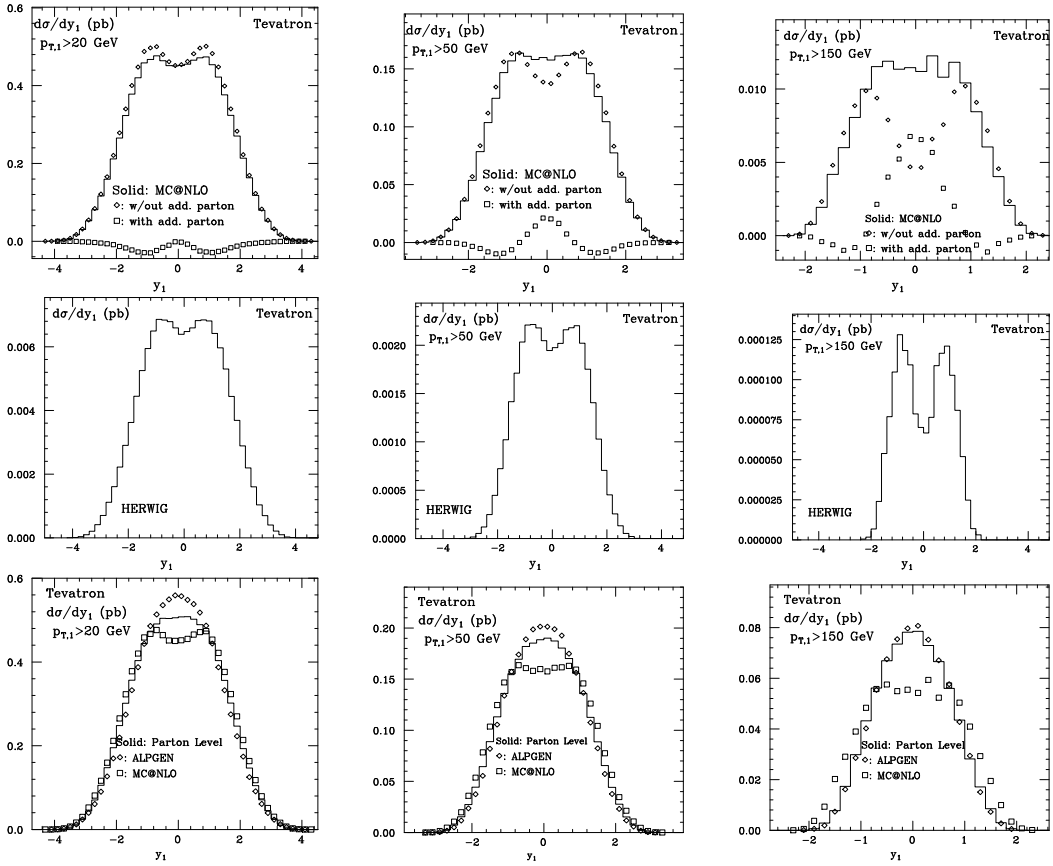

Fig. 5: Rapidity of the leading jet y_1 at Tevatron for for various jet p_T thresholds. Upper set: MC@NLO, with partial contributions. Central set: HERWIG. Lower set: comparison between ALPGEN, MC@NLO, and the parton level predictions

GEN result reproduces well the PL result, while still differing significantly from the MC@NLO distributions.

3.3 Conclusions

The analysis presented here is focused on the MC simulations of the $t\bar{t}$+jets process as predicted by ALPGEN and its matching algorithm. Several checks of that algorithm have shown its internal consistency, and pinpoint a mild dependence of the results on the parameters that define it. The consistency of the approach is then confirmed by the comparison with MC@NLO. In particular, inclusive variables show excellent agreement, once the NLO/LO K-factor is included.
Instead we found a rather surprising difference between the predictions of two codes for the rapidity distribution of the leading jet accompanying the $t\bar{t}$ pair. In view of the relevance of this variable for the study at the LHC of new physics signals, it is important to further investigate the origin of this discrepancy, with independent calculations, and with a direct comparison with data. Preliminary results obtained with the new positive-weight NLO shower MC introduced in [61–63] appear to support the distributions predicted by ALPGEN.

4 A subtraction scheme for jet cross sections at NNLO

Author: Gabor Somogyi

One of the main difficulties in performing NNLO calculations is that the finite higher-order corrections are sums of several pieces which are separately infrared (IR) divergent in $d = 4$ spacetime dimensions. To handle the IR singularities present in the intermediate stages of calculation in a general (process- and observable-independent) way is non-trivial already at NLO accuracy, where however several solutions are known [2, 3, 64–67]. It is perhaps fair to say that the most widely used is the dipole subtraction scheme of Ref. [2], which constructs a completely general and fully local approximate cross section to regularize real radiation at NLO. Setting up a general subtraction algorithm analogous to that of Ref. [2] but at NNLO accuracy has proved to be rather difficult problem. Here we give a progress report on constructing such a scheme.

4.1 Subtraction scheme at NNLO

In perturbative QCD the formal loop expansion for any production rate to NNLO accuracy reads

$$\sigma = \sigma^{\rm LO} + \sigma^{\rm NLO} + \sigma^{\rm NNLO} + \dots \,. \tag{24}$$

Let us consider $e^+e^- \to m$ jet production. Then the NNLO correction may be written as

$$\sigma^{\rm NNLO} = \int_{m+2} {\rm d}\sigma^{\rm RR}_{m+2} J_{m+2} + \int_{m+1} {\rm d}\sigma^{\rm RV}_{m+1} J_{m+1} + \int_{m} {\rm d}\sigma^{\rm VV}_{m} J_{m} \,, \tag{25}$$

i.e. it is the sum of a doubly-real, a real-virtual and a doubly-virtual contribution, each IR divergent in $d = 4$ spacetime dimensions.

The general strategy of subtraction consists of the following steps: (i) we regularize all integrals in Eq. (25) by dimensional regularization then (ii) we reshuffle the singularities between the three terms by adding and subtracting suitably defined *approximate cross sections* so that finally we rewrite Eq. (25) as

$$\sigma^{\rm NNLO} = \int_{m+2} {\rm d}\sigma^{\rm NNLO}_{m+2} + \int_{m+1} {\rm d}\sigma^{\rm NNLO}_{m+1} + \int_{m} {\rm d}\sigma^{\rm NNLO}_{m} \,, \tag{26}$$

where now each term on the right hand side is finite in $d = 4$ by construction. According to Ref. [68] we have

$$\mathrm{d}\sigma^{\mathrm{NNLO}}_{m+2} = \Big\{\mathrm{d}\sigma^{\mathrm{RR}}_{m+2} J_{m+2} - \mathrm{d}\sigma^{\mathrm{RR,A_2}}_{m+2} J_m - \Big[\mathrm{d}\sigma^{\mathrm{RR,A_1}}_{m+2} J_{m+1} - \mathrm{d}\sigma^{\mathrm{RR,A_{12}}}_{m+2} J_m\Big]\Big\}_{\varepsilon=0}, \quad (27)$$

$$\mathrm{d}\sigma^{\mathrm{NNLO}}_{m+1} = \Big\{\Big[\mathrm{d}\sigma^{\mathrm{RV}}_{m+1} + \int_1 \mathrm{d}\sigma^{\mathrm{RR,A_1}}_{m+2}\Big] J_{m+1} - \Big[\mathrm{d}\sigma^{\mathrm{RV,A_1}}_{m+1} + \Big(\int_1 \mathrm{d}\sigma^{\mathrm{RR,A_1}}_{m+2}\Big)^{\mathrm{A_1}}\Big] J_m\Big\}_{\varepsilon=0}, \quad (28)$$

and

$$\mathrm{d}\sigma^{\mathrm{NNLO}}_{m} = \Big\{\mathrm{d}\sigma^{\mathrm{VV}}_{m} + \int_2 \Big[\mathrm{d}\sigma^{\mathrm{RR,A_2}}_{m+2} - \mathrm{d}\sigma^{\mathrm{RR,A_{12}}}_{m+2}\Big] + \int_1 \Big[\mathrm{d}\sigma^{\mathrm{RV,A_1}}_{m+1} + \Big(\int_1 \mathrm{d}\sigma^{\mathrm{RR,A_1}}_{m+2}\Big)^{\mathrm{A_1}}\Big]\Big\}_{\varepsilon=0} J_m\,. \quad (29)$$

In Eq. (27) above $\mathrm{d}\sigma^{\mathrm{RR,A_1}}_{m+2}$ and $\mathrm{d}\sigma^{\mathrm{RR,A_2}}_{m+2}$ regularize the singly- and doubly-unresolved limits of $\mathrm{d}\sigma^{\mathrm{RR}}_{m+2}$ respectively. The role of $\mathrm{d}\sigma^{\mathrm{RR,A_{12}}}_{m+2}$ is two-fold: it must regularize the singly-unresolved limits of $\mathrm{d}\sigma^{\mathrm{RR,A_2}}_{m+2}$ *and* the doubly-unresolved limits of $\mathrm{d}\sigma^{\mathrm{RR,A_1}}_{m+2}$ *simultaneously*. In Eq. (28) $\mathrm{d}\sigma^{\mathrm{RV,A_1}}_{m+1}$ and $\Big(\int_1 \mathrm{d}\sigma^{\mathrm{RR,A_1}}_{m+2}\Big)^{\mathrm{A_1}}$ regularize the singly-unresolved limits of $\mathrm{d}\sigma^{\mathrm{RV}}_{m+1}$ and $\int_1 \mathrm{d}\sigma^{\mathrm{RR,A_1}}_{m+2}$ respectively.

4.2 Devising approximate cross sections

Attempting to use the known (multiple) IR factorization properties of (one-loop) squared matrix elements to devise the approximate cross sections in Eqs. (27) and (28) above, we are immediately faced with two problems. First, the various limits overlap in some regions of phase space, thus care needs to be taken to avoid multiple subtraction. Second, even once the factorization formulae are written in such a way that intersecting limits are disentangled so that multiple subtraction does not occur, the resulting expressions cannot be used as true subtraction terms because they are only defined in the strict soft and/or collinear limits. Thus, constructing the approximate cross sections proceeds in two steps: (i) we write all relevant factorization formulae in such a way that their overlap structure can be disentangled (*"matching of limits"*) and (ii) we define *"extensions"* of the formulae so that they are unambiguously defined away from the IR limits.

Let us consider first the matching of limits. A single parton, say r, can become unresolved in (i) the collinear limit, when for some hard parton $i \neq r$ we have $p_i || p_r$ and (ii) in the soft limit, when $p_r \to 0$. In these limits QCD squared matrix elements obey well-known universal factorization properties [69–72], which we exhibit below at tree level for the sake of being specific[1]

$$\mathbf{C}_{ir}|\mathcal{M}^{(0)}_{m+2}|^2 \propto \frac{1}{s_{ir}} \langle \mathcal{M}^{(0)}_{m+1}|\hat{P}^{(0)}_{ir}(z_i, k_\perp; \varepsilon)|\mathcal{M}^{(0)}_{m+1}\rangle\,, \quad (30)$$

$$\mathbf{S}_{r}|\mathcal{M}^{(0)}_{m+2}|^2 \propto \sum_{\substack{i,k \\ i\neq k}} \frac{s_{ik}}{s_{ir}s_{kr}} \langle \mathcal{M}^{(0)}_{m+1}|\boldsymbol{T}_i\boldsymbol{T}_r|\mathcal{M}^{(0)}_{m+1}\rangle\,. \quad (31)$$

To write Eqs. (30) and (31) above, we used the colour-state notation of Ref. [2] and the operator notation of taking the limits introduced in Ref. [73], while $s_{jl} = 2p_j \cdot p_l$, $(j, l = i, k, r)$, $\hat{P}^{(0)}_{ir}$

[1] To keep the discussion as simple as possible, we only indicate the structure of the factorization formulae.

are the tree-level Altarelli–Parisi splitting kernels and finally z_i is the momentum-fraction carried by parton i in the $p_{ir} \to p_i + p_r$ splitting. When parton r is both soft and collinear to the hard parton i, these limits overlap. To avoid double subtraction in this region of phase space, we must identify the common soft-collinear limit of Eqs. (30) and (31), which is found to be [73]

$$\mathbf{C}_{ir}\mathbf{S}_r|\mathcal{M}^{(0)}_{m+2}|^2 \propto \frac{1}{s_{ir}}\frac{2z_i}{1-z_i}\boldsymbol{T}_i^2|\mathcal{M}^{(0)}_{m+1}|^2\,. \tag{32}$$

Thus the formal operator

$$\mathbf{A}_1 = \sum_r \left[\sum_{i\neq r}\frac{1}{2}\mathbf{C}_{ir} + \left(\mathbf{S}_r - \sum_{i\neq r}\mathbf{C}_{ir}\mathbf{S}_r\right)\right] \tag{33}$$

counts each singly-unresolved limit precisely once and is free of double subtractions, therefore $\mathbf{A}_1|\mathcal{M}^{(0)}_{m+2}|^2$ has the same singly-unresolved singularity structure as $|\mathcal{M}^{(0)}_{m+2}|^2$ itself, *i.e.* it defines a candidate subtraction term for constructing $\mathrm{d}\sigma^{\mathrm{RR,A_1}}_{m+2}$. Similarly, applying the formal operator $\mathbf{A}_1$ to *e.g.* $2\Re\langle\mathcal{M}^{(0)}_{m+1}||\mathcal{M}^{(1)}_{m+1}\rangle$ defines a candidate subtraction term for defining $\mathrm{d}\sigma^{\mathrm{RV,A_1}}_{m+1}$, starting from the collinear [11, 74–76] and soft [77] factorization formulae for one-loop squared matrix elements.

The matching procedure is quite a bit more elaborate when two different partons, say r and s, become unresolved, which can arise in four different limits: (i) the triple collinear limit, when for some hard parton $i \neq r, s$ we have $p_i||p_r||p_s$, (ii) the doubly single collinear limit, when for two distinct hard partons $i \neq r, s$ and $j \neq r, s$ we have $p_i||p_r$ and $p_j||p_s$, (iii) the doubly soft-collinear limit, when for $i \neq r, s$ we have $p_i||p_r$ and $p_s \to 0$, and finally (iv) the double soft limit, when $p_r \to 0$ and $p_s \to 0$. The factorization formulae appropriate for each of these limits are well-known (in particular the three-parton splitting functions and the double soft gg and $q\bar{q}$ currents are given in Refs. [78–84] and Refs. [72, 85], respectively), and their highly non-trivial overlap structure was disentangled in Ref. [73]. To identify the intersection of limits, Ref. [73] computed all common limits explicitly, which is rather cumbersome. In [86], a simple and systematic procedure was proposed that leads directly to pure soft factorization formulae at any order and thus solves the problem of matching of limits in general. Finally (using the operator notation of Ref. [73]) we find that the symbolic operator

$$\begin{aligned}\mathbf{A}_2 \;=\; & \sum_r\sum_{s\neq r}\left\{\sum_{i\neq r,s}\left[\frac{1}{6}\mathbf{C}_{irs} + \sum_{j\neq i,r,s}\frac{1}{8}\mathbf{C}_{ir;js} + \frac{1}{2}\mathbf{C}\mathbf{S}_{ir;s}\right] + \frac{1}{2}\mathbf{S}_{rs} - \sum_{i\neq r,s}\left[\frac{1}{2}\mathbf{C}_{irs}\mathbf{C}\mathbf{S}_{ir;s}\right.\right. \\ & \left.\left. +\; \sum_{j\neq i,r,s}\frac{1}{2}\mathbf{C}_{ir;js}\mathbf{C}\mathbf{S}_{ir;s} + \frac{1}{2}\mathbf{C}_{irs}\mathbf{S}_{rs} + \mathbf{C}\mathbf{S}_{ir;s}\mathbf{S}_{rs} - \sum_{j\neq i,r,s}\frac{1}{2}\mathbf{C}_{ir;js}\mathbf{S}_{rs} - \mathbf{C}_{irs}\mathbf{C}\mathbf{S}_{ir;s}\mathbf{S}_{rs}\right]\right\}\end{aligned} \tag{34}$$

counts each doubly-unresolved limit precisely once (without overlaps). Thus $\mathbf{A}_2|\mathcal{M}^{(0)}_{m+2}|^2$ has the same doubly-unresolved singularity structure as $|\mathcal{M}^{(0)}_{m+2}|^2$ itself and so defines a candidate subtraction term for constructing $\mathrm{d}\sigma^{\mathrm{RR,A_2}}_{m+2}$.

Finally, we must address the matching of the singly- and doubly-unresolved limits of $|\mathcal{M}^{(0)}_{m+2}|^2$ which also overlap. $\mathrm{d}\sigma^{\mathrm{RR,A_{12}}}_{m+2}$ is introduced in Eq. (27) precisely to avoid double subtraction in the intersecting regions of phase space. However the role of this approximate cross

section is quite delicate, because (i) in the doubly-unresolved limits it must regularize $\mathrm{d}\sigma_{m+1}^{\mathrm{RR,A}_1}$, while (ii) in the singly-unresolved limits, it must regularize $\mathrm{d}\sigma_{m+2}^{\mathrm{RR,A}_2}$ *and* spurious singularities that appear in $\mathrm{d}\sigma_{m+2}^{\mathrm{RR,A}_1}$. It is thus a highly non-trivial statement that the correct candidate subtraction term can be obtained by applying the symbolic singly-unresolved operator $\mathbf{A}_1$ of Eq. (33) to $\mathbf{A}_2|\mathcal{M}_{m+2}^{(0)}|^2$ [73]. That is,

$$(\mathbf{A}_1 + \mathbf{A}_2 - \mathbf{A}_1\mathbf{A}_2)|\mathcal{M}_{m+2}^{(0)}|^2 \tag{35}$$

has the same singularity structure as $|\mathcal{M}_{m+2}^{(0)}|^2$ itself in all singly- and doubly-unresolved limits and is free of multiple subtractions.

The second step of defining the approximate cross sections calls for an extension of the limit formulae over the full phase space. As emphasized above, the candidate subtraction terms cannot yet be used as true subtraction terms because they are only well-defined in the strict limits. In order to define suitable extensions over the full phase space, we need to define momentum mappings $\{p\}_{m+2} \to \{\tilde{p}\}_{m+1}$ and $\{p\}_{m+2} \to \{\tilde{p}\}_m$ that (i) implement exact momentum conservation, (ii) lead to exact phase space factorization and (iii) respect the delicate structure of cancellations among the subtraction terms in the various limits. We find it convenient to define two types of singly-unresolved ($\{p\}_{m+2} \to \{\tilde{p}\}_{m+1}$) mappings and four types of doubly-unresolved ($\{p\}_{m+2} \to \{\tilde{p}\}_m$) mappings, corresponding to the basic types of limits that may occur (*i.e.* we define a collinear and a soft singly-unresolved mapping). The explicit forms of these momentum mappings may be found in Ref. [68] together with the full definitions of all approximate cross sections that appear in Eq. (27). The approximate cross sections in Eq. (28) are given explicitly in Refs. [87, 88].

At the risk of belabouring the point, we note again that all our momentum mappings lead to an exact factorization of the phase space in the symbolic form

$$\mathrm{d}\phi_{m+2} = \mathrm{d}\phi_{m+1}[\mathrm{d}p_1] \qquad \text{and} \qquad \mathrm{d}\phi_{m+2} = \mathrm{d}\phi_m[\mathrm{d}p_2]\,, \tag{36}$$

thus the singular integrals of the subtraction terms over the phase space of the unresolved parton(s) can be computed once and for all, independent of the jet function and the rest of the phase space integration.

4.3 Conclusions

We have set up a general (process- and observable-independent) subtraction scheme for computing QCD jet cross sections at NNLO accuracy for processes with no coloured particles in the initial state. Our scheme can naturally be viewed as the generalization of the dipole subtraction scheme of Ref. [2] to NNLO. We have defined all approximate cross sections needed to regularize the $m+2$ and $m+1$ parton contributions (*i.e.* all terms in Eqs. (27) and (28)) explicitly. Our subtraction terms are *fully local*, *i.e.* all colour and azimuthal correlations are properly taken into account. Thus we can check the convergence of our subtraction terms to the doubly-real, or real-virtual cross sections in any unresolved limit explicitly. In addition, we have checked that the regularized doubly-real and real-virtual contributions to $e^+e^- \to 3$ jet production are finite by computing the first three moments of the thrust and C-parameter distributions, see Tab. 1. In order to finish the definition of the subtraction scheme, one must still compute the singly- and doubly-unresolved integrals of the approximate cross sections that appear in Eq. (29). All

n	$\langle(1-t)^n\rangle_{\rm RV}/10^1$	$\langle C^n\rangle_{\rm RV}/10^1$	$\langle(1-t)^n\rangle_{\rm RR}$	$\langle C^n\rangle_{\rm RR}$
1	123 ± 1	433 ± 5	-92.7 ± 3.4	-344 ± 14
2	25.5 ± 0.2	325 ± 2	-3.07 ± 0.43	-142 ± 3
3	4.79 ± 0.03	180 ± 1	2.01 ± 0.12	6.29 ± 1.87

Table 1: The real-virtual and doubly-real contributions to the first three moments of the thrust and C-parameter distribution in $e^+e^- \to 3$ jets.

singly-unresolved integrals (denoted by $\int_1$ in Eqs. (28) and (29) above) have recently been computed [87, 89–91] and we expect that the techniques applied will be flexible enough to compute the doubly-unresolved integrals (denoted by $\int_2$ in Eq. (29)) as well. This is work in progress.

We are grateful to our collaborators: U. Aglietti, P. Bolzoni, V. Del Duca, C. Duhr and S. Moch. This work was supported in part by Hungarian Scientific Research Fund grant OTKA K-60432 and by the Swiss National Science Foundation (SNF) under contract 200020-117602.

References

[1] R. K. Ellis, D. A. Ross, and A. E. Terrano, Nucl. Phys. **B178**, 421 (1981).

[2] S. Catani and M. H. Seymour, Nucl. Phys. **B485**, 291 (1997), arXiv:hep-ph/9605323.

[3] S. Frixione, Z. Kunszt, and A. Signer, Nucl. Phys. **B467**, 399 (1996), arXiv:hep-ph/9512328.

[4] E. W. N. Glover, Nucl. Phys. Proc. Suppl. **116**, 3 (2003), arXiv:hep-ph/0211412.

[5] W. T. Giele and E. W. N. Glover, JHEP **04**, 029 (2004), arXiv:hep-ph/0402152.

[6] R. K. Ellis, W. T. Giele, and G. Zanderighi, Phys. Rev. **D73**, 014027 (2006), arXiv:hep-ph/0508308.

[7] A. Denner and S. Dittmaier, Nucl. Phys. **B734**, 62 (2006), arXiv:hep-ph/0509141.

[8] T. Binoth, J. P. Guillet, G. Heinrich, E. Pilon, and T. Reiter (2008), arXiv:0810.0992 [hep-ph].

[9] W. Giele, E. W. N. Glover, and G. Zanderighi, Nucl. Phys. Proc. Suppl. **135**, 275 (2004), arXiv:hep-ph/0407016.

[10] NLO Multileg Working Group Collaboration, Z. Bern *et al.* (2008), arXiv:0803.0494 [hep-ph].

[11] Z. Bern, L. J. Dixon, D. C. Dunbar, and D. A. Kosower, Nucl. Phys. **B425**, 217 (1994), arXiv:hep-ph/9403226.

[12] R. Britto, F. Cachazo, and B. Feng, Nucl. Phys. **B725**, 275 (2005), arXiv:hep-th/0412103.

[13] C. F. Berger, Z. Bern, L. J. Dixon, D. Forde, and D. A. Kosower, Phys. Rev. **D75**, 016006 (2007), arXiv:hep-ph/0607014.

[14] C. F. Berger *et al.*, Phys. Rev. **D78**, 036003 (2008), arXiv:0803.4180 [hep-ph].

[15] R. K. Ellis, W. T. Giele, and Z. Kunszt, JHEP **03**, 003 (2008), arXiv:0708.2398 [hep-ph].

[16] W. T. Giele, Z. Kunszt, and K. Melnikov, JHEP **04**, 049 (2008), arXiv:0801.2237 [hep-ph].

[17] W. T. Giele and G. Zanderighi, JHEP **06**, 038 (2008), arXiv:0805.2152 [hep-ph].

[18] G. Ossola, C. G. Papadopoulos, and R. Pittau, Nucl. Phys. **B763**, 147 (2007), arXiv:hep-ph/0609007.

[19] Z. Bern and D. A. Kosower, Nucl. Phys. **B362**, 389 (1991).

[20] F. Berends and W. Giele, Nucl. Phys. **B306**, 759 (1988).

[21] Z. Bern, L. J. Dixon, D. C. Dunbar, and D. A. Kosower, Nucl. Phys. **B435**, 59 (1995), arXiv:hep-ph/9409265.

[22] R. K. Ellis and G. Zanderighi, JHEP **02**, 002 (2008), arXiv:0712.1851 [hep-ph].

[23] R. K. Ellis, W. T. Giele, and G. Zanderighi, JHEP **05**, 027 (2006), arXiv:hep-ph/0602185.

[24] D. Forde and D. A. Kosower, Phys. Rev. **D73**, 061701 (2006), arXiv:hep-ph/0509358.

[25] R. Kleiss, W. J. Stirling, and S. D. Ellis, Comput. Phys. Commun. **40**, 359 (1986).

[26] V. Del Duca, W. Kilgore, C. Oleari, C. Schmidt, and D. Zeppenfeld, Nucl. Phys. **B616**, 367 (2001), arXiv:hep-ph/0108030.

[27] R. Kleiss and H. Kuijf, Nucl. Phys. **B312**, 616 (1989).

[28] R. K. Ellis, W. T. Giele, Z. Kunszt, and K. Melnikov (2008), arXiv:0806.3467 [hep-ph].

[29] R. K. Ellis, W. T. Giele, Z. Kunszt, K. Melnikov, and G. Zanderighi (2008), arXiv:0810.2762 [hep-ph].

[30] S. Catani. Presented at the Workshop HP^2: High Precision for Hard Processes at the LHC, Sept. 2006, Zurich, Switzerland.

[31] T. Gleisberg. Ph.D. Thesis, University of Dresden. .

[32] S. Catani, T. Gleisberg, F. Krauss, G. Rodrigo, and J.-C. Winter, JHEP **09**, 065 (2008), arXiv:0804.3170 [hep-ph].

[33] R. Feynman, Acta Phys. Polon. **24**, 697 (1963).

[34] M. Mangano and S. Parke, Phys. Rept. **200**, 301 (1991), arXiv:hep-th/0509223.

[35] F. Caravaglios and M. Moretti, Phys. Lett. **B358**, 332 (1995), arXiv:hep-ph/9507237.

[36] R. K. P. Draggiotis and C. Papadopoulos, Phys. Lett. **B439**, 157 (1998), arXiv:hep-ph/9807207.

[37] R. K. P. Draggiotis and C. Papadopoulos, Eur. Phys. J. **C24**, 447 (2002), arXiv:hep-ph/0202201.

[38] P. S. F. Cachazo and E. Witten, JHEP **09**, 006 (2004), arXiv:hep-th/0403047.

[39] F. C. R. Britto and B. Feng, Nucl. Phys. **B715**, 499 (2005), arXiv:hep-th/0412308.

[40] B. F. R. Britto, F. Cachazo and E. Witten, Phys. Rev. Lett. **94**, 181602 (2005), arXiv:hep-th/0501052.

[41] D. Soper, Phys. Rev. Lett. **81**, 2638 (1998), arXiv:hep-ph/9804454.

[42] M. Kramer and D. E. Soper, Phys. Rev. **D66**, 054017 (2002), arXiv:hep-ph/0204113.

[43] T. Kleinschmidt. DESY-THESIS-2007-042.

[44] M. Moretti, F. Piccinini, and A. D. Polosa (2008), arXiv:0802.4171 [hep-ph].

[45] R. K. S. Catani, F. Krauss and B. Webber, JHEP **11**, 063 (2001).

[46] L. Lonnblad, JHEP **05**, 046 (2002).

[47] F.Krauss, JHEP **08**, 015 (2002).

[48] S. Hoche *et al.* (2006). hep-ph/0602031.

[49] M. Mangano (2002). www-cpd.fnal.gov/personal/mrenna/tuning/nov2002/mlm.pdf.

[50] M. L. Mangano, M. Moretti, F. Piccinini, and M. Treccani, JHEP **01**, 013 (2007), arXiv:hep-ph/0611129.

[51] J. Alwall *et al.*, Eur. Phys. J. **C53**, 473 (2008).

[52] M. L. Mangano, M. Moretti, F. Piccinini, R. Pittau, and A. D. Polosa, JHEP **07**, 001 (2003), arXiv:hep-ph/0206293.

[53] S. Frixione and B. R. Webber, JHEP **06**, 029 (2002), hep-ph/0204244.

[54] S. Frixione, P. Nason, and B. R. Webber, JHEP **08**, 007 (2003), hep-ph/0305252.

[55] S. Frixione and B. Webber (2006). The MC@NLO 3.2 event generator, hep-ph/0601192.

[56] G. Marchesini and B. Webber, Nucl. Phys. **B310**, 461 (1988).

[57] G. Marchesini *et al.*, Comput. Phys. Commun. **67**, 465 (1992).

[58] G. Corcella *et al.*, JHEP **01**, 010 (2001), arXiv:hep-ph/0011363.

[59] W. S. A.D. Martin, R.G. Roberts and R. Thorne, Eur. Phys. J. **C23**, 73 (2002).

[60] E. Paige and S. Protopopescu. Physics of the SSC, in Snowmass, 1986, Colorado, edited by R. Donaldson and J. Marx.

[61] P. Nason, JHEP **11**, 040 (2004), hep-ph/0409146.

[62] P. Nason and G. Ridolfi, JHEP **0608**, 077 (2006).

[63] C. O. S. Alioli, P. Nason and E. Re, JHEP **07**, 060 (2008).

[64] W. T. Giele and E. W. N. Glover, Phys. Rev. **D46**, 1980 (1992).

[65] W. T. Giele, E. W. N. Glover, and D. A. Kosower, Nucl. Phys. **B403**, 633 (1993), arXiv:hep-ph/9302225.

[66] Z. Nagy and Z. Trócsányi, Nucl. Phys. **B486**, 189 (1997), arXiv:hep-ph/9610498.

[67] S. Frixione, Nucl. Phys. **B507**, 295 (1997), arXiv:hep-ph/9706545.

[68] G. Somogyi, Z. Trócsányi, and V. Del Duca, JHEP **01**, 070 (2007), arXiv:hep-ph/0609042.

[69] J. Frenkel and J. C. Taylor, Nucl. Phys. **B116**, 185 (1976).

[70] D. Amati, R. Petronzio, and G. Veneziano, Nucl. Phys. **B146**, 29 (1978).

[71] A. Bassetto, M. Ciafaloni, and G. Marchesini, Phys. Rept. **100**, 201 (1983).

[72] S. Catani and M. Grazzini, Nucl. Phys. **B570**, 287 (2000), arXiv:hep-ph/9908523.

[73] G. Somogyi, Z. Trócsányi, and V. Del Duca, JHEP **06**, 024 (2005), arXiv:hep-ph/0502226.

[74] Z. Bern, V. Del Duca, and C. R. Schmidt, Phys. Lett. **B445**, 168 (1998), arXiv:hep-ph/9810409.

[75] D. A. Kosower and P. Uwer, Nucl. Phys. **B563**, 477 (1999), arXiv:hep-ph/9903515.

[76] Z. Bern, V. Del Duca, W. B. Kilgore, and C. R. Schmidt, Phys. Rev. **D60**, 116001 (1999), arXiv:hep-ph/9903516.

[77] S. Catani and M. Grazzini, Nucl. Phys. **B591**, 435 (2000), arXiv:hep-ph/0007142.

[78] A. Gehrmann-De Ridder and E. W. N. Glover, Nucl. Phys. **B517**, 269 (1998), arXiv:hep-ph/9707224.

[79] J. M. Campbell and E. W. N. Glover, Nucl. Phys. **B527**, 264 (1998), arXiv:hep-ph/9710255.

[80] S. Catani and M. Grazzini, Phys. Lett. **B446**, 143 (1999), arXiv:hep-ph/9810389.

[81] D. A. Kosower, Nucl. Phys. **B552**, 319 (1999), arXiv:hep-ph/9901201.

[82] V. Del Duca, A. Frizzo, and F. Maltoni, Nucl. Phys. **B568**, 211 (2000), arXiv:hep-ph/9909464.

[83] D. A. Kosower, Phys. Rev. **D67**, 116003 (2003), arXiv:hep-ph/0212097.

[84] D. A. Kosower, Phys. Rev. Lett. **91**, 061602 (2003), arXiv:hep-ph/0301069.

[85] F. A. Berends and W. T. Giele, Nucl. Phys. **B313**, 595 (1989).

[86] Z. Nagy, G. Somogyi, and Z. Trócsányi (2007), arXiv:hep-ph/0702273.

[87] G. Somogyi and Z. Trócsányi, Acta Phys. Chim. Debr. **XL**, 101 (2006), arXiv:hep-ph/0609041.

[88] G. Somogyi and Z. Trócsányi, JHEP **01**, 052 (2007), arXiv:hep-ph/0609043.

[89] G. Somogyi and Z. Trócsányi, JHEP **08**, 042 (2008), arXiv:0807.0509 [hep-ph].

[90] U. Aglietti, V. Del Duca, C. Duhr, G. Somogyi, and Z. Trócsányi (2008), arXiv:0807.0514 [hep-ph].

[91] P. Bolzoni, S. Moch, G. Somogyi, and i. p. Trócsányi, Z. (in preparation), arXiv:?? [hep-ph].